Understanding precursor-derived amorphous Si-C-N ceramics on the atomic scale

Marc Amkreutz* and Thomas Frauenheim
Theoretische Physik, FB6, Universität Paderborn, Warburger Str. 100, D-33098 Paderborn, Germany
(Received 28 September 2001; revised manuscript received 10 January 2002; published 26 March 2002)

The atomic structure of a precursor-derived amorphous ceramic with the composition $Si_{37}C_{32}N_{31}$ and a density of 2.4 g/cm^3 was modeled using a density-functional-based molecular dynamics simulation. Three different model structures were generated, and their total structure factors and total pair correlation functions from x-ray and neutron diffraction were calculated. For two of them, these data were found to agree very well with the experimental results. The different atomic structures of these two models could only be distinguished by the calculated partial pair correlation functions and their infrared spectra. It could be shown that in the final ceramic a phase separation into amorphous Si_3N_4, amorphous SiC, and graphitelike amorphous carbon has to appear.

DOI: 10.1103/PhysRevB.65.134113 PACS number(s): 61.43.Bn, 81.05.Je

I. INTRODUCTION

Since the introduction of the polymer-to-ceramic conversion processing route, a lot of difficulties in ceramics production resulting from the former used sintering technique could be avoided.[1,2] For sintering of ceramic powders, sintering aids had to be used to enhance densification. But because of the segregation of the sintering aids at the grain boundaries, these led to pores or cracks in the material at higher temperatures together with a shrinkage of up to 15%–20%. Instead, for the polymer-ceramic conversion, organometallic polymer precursors like polycarbosilane, -silazane, and -siloxane can be used to prepare ceramic components at low temperatures and without the addition of sintering aids by thermally induced composition (pyrolysis). Therefore, several plastic shaping technologies and laminated object manufacturing techniques can be applied to the preceramic polymers before pyrolysis, preventing expensive postprocessing steps of the final ceramic.[2]

With different precursors and varying pyrolysis regimes a wide range of amorphous ceramics with various compositions have been obtained, especially in the ternary phase diagram of Si-C-N.[1,3–6] Amorphous ceramics produced in this way have high-temperature stability, strain and oxidation resistance[1,7] and are used as coatings for tools, turbines, or engines and as ceramic fibers to reinforce ceramic matrix composites (CMC) in air- and spacecraft structures.[2]

A variety of experimental techniques, like x-ray and neutron diffraction,[3,4,6] nuclear magnetic resonance (NMR),[5] transmission electron microscopy (TEM), and electron spectroscopic imaging (ESI),[8] have been applied to understand the polymer-to-ceramic conversion and to characterize the structure of the produced ceramics. This is necessary for the generation and understanding of the special high-temperature stability of the ceramics.

But in spite of these experimental efforts, the detailed atomic structure of these ceramics and so the exact relation between used precursor, pyrolysis regime, and resulting properties of the final ceramic material are still not well known. For example, it is still a question whether there is a homogeneous distribution of the carbon throughout the whole structure or if a separate amorphous carbon phase exists and of what kind the local environment of the different atom types is.

At this point, computer simulations at atomic level of these amorphous Si-C-N ceramics are highly desirable for their understanding because they are able to answer these questions, delivering direct insight into the amorphous structure and providing correlations between structure and physical properties.

However, there have been only two theoretical approaches up to now. The one has been a Reverse Monte Carlo (RMC) method[9] applied by Dürr *et al.*[6] to obtain the amorphous structure starting from the experimental total structures factors from neutron and x-ray scattering. The other has been a molecular dynamics (MD) simulation based on classical many-body Tersoff potentials[10] used by Matsunaga *et al.*[11] to generate an amorphous Si-C-N ceramic. It is noteworthy that both methods used some kind of constraints for the simulation. In the RMC simulation, additional information about a phase separation was employed by using coordination constraints, while for the Tersoff potential MD, the formation of N-N and C-N pairs was totaly prevented from the very beginning.

Our approach is a density-functional-theory- (DFT-) based molecular dynamics simulation of a ternary ceramic system. In contrast to MD with empirical potentials, here the interatomic forces are calculated on a quantum mechanical basis without any constraints regarding coordination or bonding. Such a simulation becomes highly desirable to especially improve the atomic scale and local environment understanding of structure formation and related property correlations. In closely correlating the modeling and experimental efforts, it may become possible to exactly tailor a material for a certain application just by choosing the right precursor and pyrolysis regime at the beginning.

II. COMPUTATIONAL APPROACH: STRUCTURE SIMULATION

For the generation of the structure of the amorphous ceramics we used MD simulations. The necessary interatomic forces are obtained from the density-functional-based tight-binding (DFTB) scheme described in detail elsewhere.[12–15]

Compared to standard tight-binding methods, in the DFTB scheme the Hamiltonian and overlap matrices and the repulsive potential of the atomic interaction are calculated within a two-center approach to density functional theory.

In this study we focus on an amorphous ceramic produced and examined by x-ray and neutron diffraction by Schempp *et al.*[3] This ceramic was obtained by pyrolysis of a polyhydromethylsilazane polymer (NCP 200, Nichimen Corporation, Japan) with formula $[(CH_3)_2SiNH]_x[CH_3SiHNH]_y[CH_3SiN]_z$ and $x \approx y+z \approx 0.5$.[1] The material was pyrolyzed at 1050 °C in an argon atmosphere without any previous crosslinking and densification of the precursor polymer, yielding an amorphous ceramic with the composition $Si_{37}C_{32}N_{31}$ and a density of 2.4 g/cm^3.

The composition and density served as the only input parameters for the generation of the ceramics by MD. The total atom number, subdivided into the three atomic types correspondingly to the composition, were enclosed within a periodic supercell with fixed volume according to the given microscopic mass density of 2.4 g/cm^3. The atomic arrangement of the different starting structures of the models was chosen according to experimental suggestions; see Sec. IV.

To simulate the pyrolysis process we have applied a simulated annealing MD with constant number of particles N and constant volume V. The model system was first heated from 300 K to 1000 K for 1 ps with linear increase of the temperature. Afterwards, the structure was equilibrated at 1000 K for 1 ps, followed by a cooling down to 300 K again in 1 ps and a final equilibration at this temperature for another 1 ps. The equations of motion of the atoms were integrated using a Verlet algorithm with a time interval of 1 fs. Finally, a conjugate gradient was used to optimize the structure and minimize the total energy.

The maximum temperature of the MD is chosen according to experimental conditions in order to at least partly preserve precursor characteristics which is desirable for these precursor-derived amorphous ceramics.

III. DIFFRACTION THEORY: THE OTHER WAY AROUND

When investigating an amorphous structure by x-ray and neutron diffraction one obtains the total structure factor $S(q)$ of the material from the coherently scattered intensity, using, for example, the approach of Faber and Ziman,[16] where $q = 4\pi \sin(\theta)/\lambda$ is the wave vector transfer and 2θ the scattering angle. Fourier transformation of this total structure factor yields the total pair correlation function or reduced radial distribution function

$$G(r) = \frac{2}{\pi}\int_0^\infty q[S(q)-1]\,\sin(qr)dq, \tag{1}$$

which consists of the sum of the partial pair correlation functions $G_{ij}(r)$ with weighting factors W_{ij} corresponding to the composition of the material and the scattering method:

$$G(r) = \sum_{i=1}^{n}\sum_{j=1}^{n} W_{ij}G_{ij}(r). \tag{2}$$

Here, n is the number of atom types of the system. Only this function provides information about the real-space structure of the material as bond lengths or bond angles.

For perfect transformation, $S(q)$ must be known for an infinite range of q values. This is obviously not the case in practice, where only a limited range up to a $q_{\max}$ can be measured. Thus, transformation leads to so-called truncation errors in $G(r)$, causing a loss in resolution and termination ripples, which decay with increasing radius.[17] These can be alleviated by introducing a damping factor $D(q)$ which is multiplied by the kernel of Eq. (1). Different functions are used for this, but the most favorable is that due to Lorch which reduces the ripples more rapidly:[18]

$$D_{\text{Lorch}}(q) = \frac{q_{\max}}{\pi q}\,\sin\left(\frac{\pi q}{q_{\max}}\right). \tag{3}$$

From the theoretical point of view, it is just the other way around. Knowing the atomic structure, the partial pair correlation functions result from the histograms $H_{ij}(r)$ of the distances of all atom pairs of the model with the histogram stepwidth Δr (Ref. 19):

$$G_{ij}(r) = \frac{H_{ij}(r)}{r\Delta r x_j} - 4\pi\rho_{\text{T}} r. \tag{4}$$

Here, x_j is the concentration of the atom type j and $\rho_{\text{T}} = N/V$ is the particle density. Applying Eq. (2) gives the total pair correlation function of the system, and Fourier transformation leads to the total structure factor

$$S(q) = 1 + \int_0^\infty G(r)\,\frac{\sin(qr)}{q}\,dr. \tag{5}$$

To take into account the damping function used in experiment to reduce the termination ripples, this $S(q)$ is again transformed according to Eq. (1) with the corresponding damping factor $D(q)$. This yields a damped total pair correlation function $G_{\text{D}}(r)$ that can be compared to the experimental one.

IV. RESULTS AND DISCUSSION

A. Homogeneous amorphous model

The first amorphous model (the homogeneous amorphous model HA) was created by the MD simulation described above, using a NCP 200-like precursor structure with 240 atoms and given composition and density as starting structure. This means that from the beginning the different atoms have been arranged accordingly to the stoichiometry of NCP 200 but without any hydrogen.

In this way, we obtained an amorphous structure of which the periodic supercell is shown in Fig. 1. One can see that the carbon atoms (black spheres) are distributed homogeneously throughout the whole structure, preferring bonding to Si atoms, but also C-C- and C-N-bonds occur. The model is con-

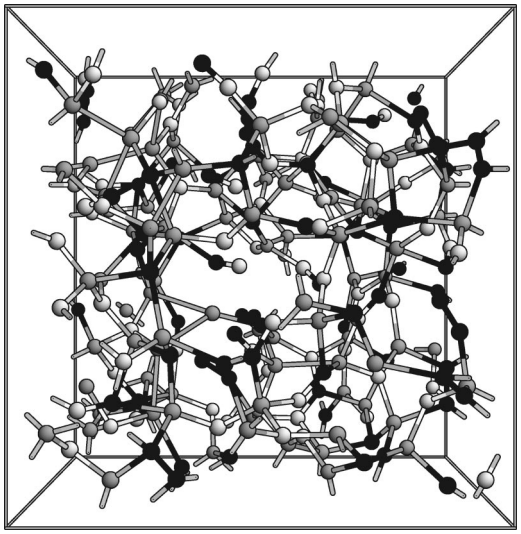

FIG. 1. Structure of the homogeneous amorphous model HA. Carbon atoms are shown as black spheres, silicon as dark gray ones, and nitrogen as white ones.

sistent with Uhlig *et al.* suggesting the possibility of a homogeneous distribution of carbon throughout the structure for another NCP 200-derived ceramic with composition $Si_{40}C_{24}N_{36}$.[4] It is worth mentioning that in all our studies the simulated pyrolysis of NCP 200-like polymer precursor structures always yielded a homogenous distribution of atom types throughout the model.[27]

Comparing the coordination numbers and bond lengths given in Table I, it is obvious that the bond lengths of Si-N and C-C are in good agreement with the experimental findings, while that of Si-C is slightly overestimated, but coordination numbers strongly deviate. Silicon is surrounded by as much nitrogen as carbon which is but only half the amount as found in experiment. In addition, the total coordination number of nitrogen is too small due to the appearance of terminating nitrogen atoms in the structure. One of this can be seen right in the center of Fig. 1.

The structural discrepancy reveals itself even more in the total structure factors displayed in Fig. 2. Although the peak positions of the calculated structure factors match already well with the ones obtained from x-ray and neutron scattering, the intensity of the peaks is too small, especially for the two main peaks below 6 $Å^{-1}$. As a consequence, a similar

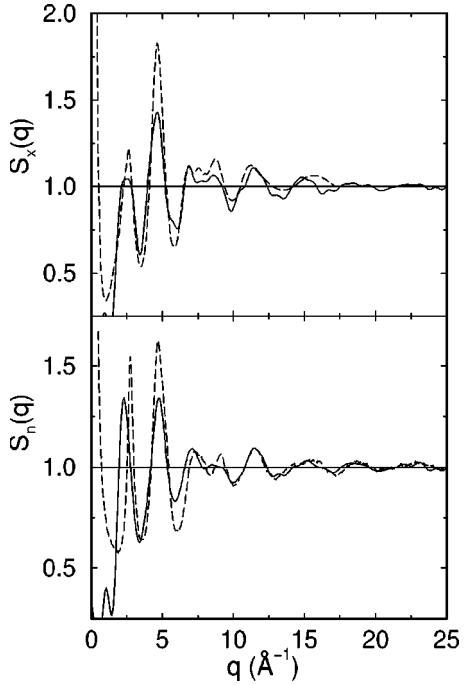

FIG. 2. Calculated total structure factors of the homogeneous amorphous model HA (solid line) and experimental ones of the ceramic produced by Schempp *et al.* (Ref. 3) (dashed line) from x-ray (upper panel) and neutron (lower panel) diffraction.

effect can be observed for the total pair correlation function $G(r)$, of which the intensity of the main peaks describing the first- and second-neighbor correlations is considerably too small.

Regarding these results, a different atomic and structural arrangement in the model is necessary to improve the coordination numbers and the lack of intensity in the structure factor and pair correlation function.

B. Phase-separated clustered amorphous model

Regarding the coordination numbers k_{SiC} and k_{SiN} of the experimental ceramic, it is not possible to decide whether there exist only SiN_4 and SiC_4 tetrahedra or if also mixed tetrahedra $Si(CN)_4$ occur in the structure. Assuming the nonexistence of such mixed tetrahedra, which was supported by small-angle scattering examination of the ceramic, Schempp

TABLE I. Coordination numbers and selected bond lengths of the homogeneous amorphous model HA, the phase-separated clustered model PSC, and the phase-separated layered model PSL compared to the experimental data (Ref. 3).

	Experimental	HA	PSC	PSL
$k_{SiSi}:k_{SiC}:k_{SiN}$	0.0:1.0:3.0	0.4:1.6:1.7	0.1:1.2:2.4	0.0:1.4:2.4
$k_{CSi}:k_{CC}:k_{CN}$	1.2:—:—	1.9:0.4:0.4	1.3:1.5:0.0	1.5:1.4:0.0
$k_{NSi}:k_{NC}:k_{NN}$	3.6:—:—	1.9:0.4:0.0	2.8:0.0:0.0	2.8:0.0:0.0
$R_{Si\text{-}N}$ [Å]	1.74±0.10	1.73±0.03	1.74±0.03	1.76±0.03
$R_{Si\text{-}C}$ [Å]	1.83±0.09	1.97±0.16	1.99±0.17	1.99±0.16
$R_{C\text{-}C}$ [Å]	1.37	1.34±0.12	1.40±0.09	1.41±0.11

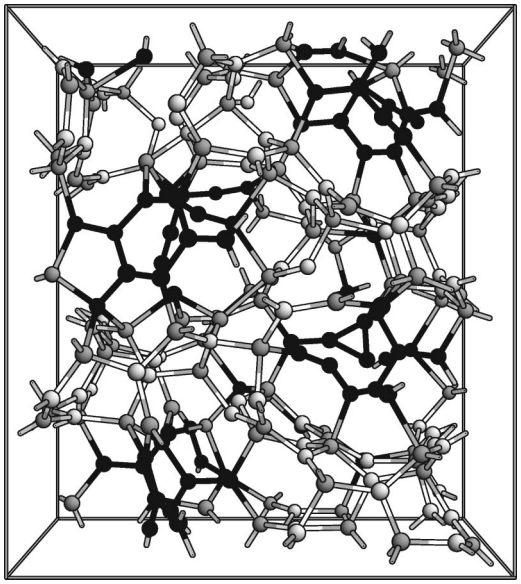

FIG. 3. Structure of the phase-separated clustered amorphous model PSC. Carbon atoms are shown as black spheres, silicon as dark gray ones, and nitrogen as white ones.

et al. suggested a phase separation into amorphous Si_3N_4, SiC, and graphitelike amorphous carbon.[3] Acting on this suggestion and keeping in mind that starting with a NCP 200-like precursor structure always yields a homogeneous distribution of atoms as mentioned before, the precursor structure now is constructed differently. For the second amorphous model we are starting out from a C_3N_4 crystal suggested by Teter and Hemley[20] in which first all of the carbon atoms were substituted by silicon while after that carbon atoms were incorporated in order to form small carbon-rich domains from the very beginning. This proceeding has also been motivated by the fact that after further heating of the amorphous ceramic crystallization takes place. The model structure consists of 224 atoms in the periodic supercell having the same composition and density as our first model, HA.

Applying the same MD scheme as before, we obtained the amorphous ceramic shown in Fig. 3. The carbon atoms are clustered together and form twisted π-bonded ringlike structures, particularly sixfold rings, which are connected to the rest of the network by silicon atoms forming a low concentration SiC phase. This, at least, is surrounded by almost only amorphous SiN_4 tetrahedra. Also three-fold-coordinated silicon appears in the structure, leading to an average coordination number of silicon less than 4. This is not uncommon for amorphous materials including silicon.[21,22]

The model is as well consistent with the detection of Si-C bonds in NMR experiments by Gaskell[23] and Seitz *et al.*[5] as is the homogeneous model HA. But the three different Si sites SiN_2C_2, SiN_3C, and SiN_4 reported by Seitz *et al.*[5] in their amorphous NCP 200-derived material only appear in this phase-separated clustered amorphous model (PSC) while in the model HA no SiN_4 site is present at all due to the homogenous distribution of atom types.

Looking at the bond lengths and coordination numbers (see Table I), the bond lengths of this model are still in good agreement with the experiment, again with a slight overestimation of the Si-C bond length. But in comparison to the homogeneous amorphous model HA, all coordination numbers now have improved significantly towards the experimental data. However, k_{SiN} and k_{NSi} are still too small, a fact that will be discussed later on.

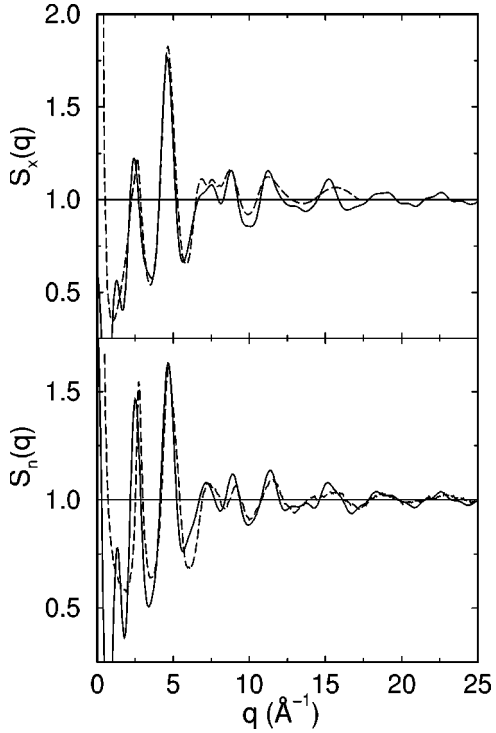

FIG. 4. Calculated total structure factors of the phase-separated clustered amorphous model PSC (solid line) and experimental ones of the ceramic produced by Schempp *et al.* (Ref. 3) (dashed line) from x-ray (upper panel) and neutron (lower panel) diffraction.

The total structure factors for the PSC model are given in Fig. 4. This time, not only the peak positions, but also the peak heights are in very good agreement with the experimental structure factors. As a new feature, a small peak at approximately $q=1.7$ Å^{-1} appears and for S_n a steep rise of the structure factor towards small q values occurs. But in this case, it is no small-angle scattering effect, i.e., a sign of a phase separation, which is indicated by this rise of the structure factor in the corresponding experimental data. The behavior of the calculated function below $q\approx 2$ Å^{-1} is artificial and due to the limited cell lengths of the periodic supercell. In the simulation, atomic correlations larger than half the minimum of this cell lengths are disturbed by the periodicity and are not chararcteristic for the amorphous structure anymore.[24] Hence, the area $q<2$ Å^{-1} of the structure factors must not be taken into account and small-angle scattering effects are not included. Nevertheless, considering the functions from $q=2$ Å^{-1} on, the calculated ones match the experimental ones very well.

Fourier transformation of the structure factors with Lorch damping with $q_{\mathrm{max}}=25$ Å^{-1} for neutron scattering and $q_{\mathrm{max}}=18$ Å^{-1} for x rays according to the experiment gave the total pair correlation functions shown in Fig. 5. The overall profile and peak positions agree well with the experimen-

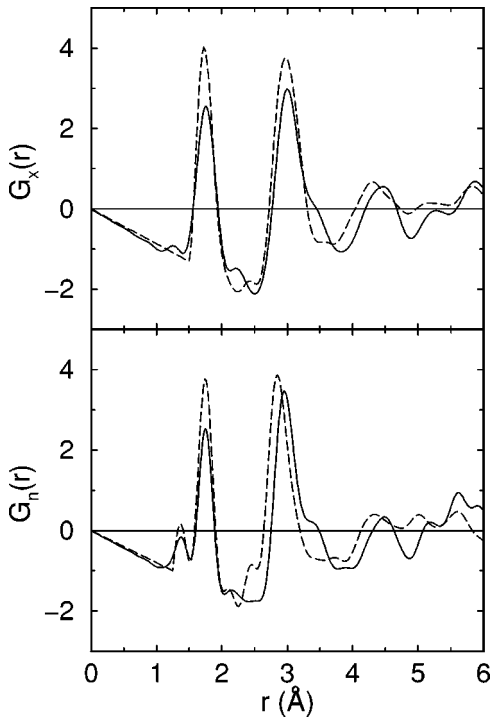

FIG. 5. Calculated total pair correlation function of the phase-separated clustered amorphous model PSC (solid line) and experimental ones of the ceramic produced by Schempp *et al.* (Ref. 3) (dashed line) from x-ray (upper panel) and neutron (lower panel) diffraction.

tal results. Only the intensities of the peaks below $r=2$ Å are a little too small due to the damping.

Considering the weighting factors (see Table II) and the corresponding distances in crystalline Si_3N_4 and SiC,[25,26] Schempp *et al.* asigned the peaks at 1.74 Å of the experimental $G_x(r)$ and $G_n(r)$ mainly to a Si-N correlation and a small contribution of Si-C bonds at 1.83 Å. In the same way, they attributed the peak at 2.98 Å in $G_x(r)$ to Si-(N)-Si, and the ones at 1.37 Å and 2.85 Å in $G_n(r)$ to a C-C and a N-(Si)-N correlation, respectively.

To have a closer look at this assignments, we calculated the partial pair correlation functions $G_{ij,x}(r)$ and $G_{ij,n}(r)$ of the amorphous structure, given in Fig. 6. The first peak of the total pair correlation functions at 1.38 Å consists of a C-C correlation at 1.40 Å and the tail of the Si-N peak centered at 1.74 Å. The oscillation of this tail at 1.40 Å is the reason for the left shift of the total pair correlation function peak to 1.38 Å. Therefore, this first peak can be attributed to C-C bonds almost only, the different height explained by the different weighting factors for x-ray and neutron diffraction. This is in good agreement with the bond length of 1.42 Å in graphite. But the second peak at 1.75 Å includes contributions from Si-N, Si-C, and C-C bonds. Here, the tail of the C-C correlation gives only a small contribution to the total function because of the small weighting factor. But nevertheless, it is responsible for the right shift of the Si-C peak in comparisson to the experimental data, in which the C-C peak was not taken into account. This explains the difference in the bond length of Si-C suggested by Schempp *et al.* and the calculated one (see Table I).

TABLE II. Weighting factors W_{ij} of the partial pair correlation functions of the amorphous models PSC and PSL, and experimental ones (Ref. 3) from x-ray and neutron diffraction.

		W_{SiSi}	W_{SiN}	W_{SiC}	W_{NN}	W_{NC}	W_{CC}
PSC/PSL	x	0.32	0.24	0.24	0.05	0.10	0.05
Experiment	x	0.312	0.262	0.231	0.055	0.097	0.043
PSC/PSL	n	0.05	0.20	0.14	0.20	0.28	0.11
Experiment	n	0.055	0.206	0.153	0.193	0.287	0.106

However, the peak in the total function results mainly from the Si-N bonds having the largest contribution with respect to the corresponding W_{ij}. The small peak at 2.15 Å in $G_n(r)$ which still belongs to the first-neighbor correlation is a combination of long Si-C and Si-N bonds. The next peak at 2.95 Å in $G_n(r)$, the first one of the next-nearest-neighbor correlation that begins at 2.4 Å, is made up of N-N, Si-Si, and C-N correlations at 2.91 Å, 3.00 Å, and 3.04 Å, respectively. This is in good consistency with the coordination numbers of k_{SiSi}, k_{CN}, and k_{NN} being almost zero. Taking into account the weighting factors in Table II, the main contribution is that of N-N, the other two just causing a little shift to the right of this peak in the total function. For $G_x(r)$ it is almost the same with the peak at 3.00 Å, with the only difference in the large x-ray weighting factor $W_{SiSi}=0.32$, making the Si-Si correlation the most important contribution.

Another fact should be mentioned regarding the partial pair correlation functions and the coordination number k_{SiN} and k_{NSi}. The intensities of the main peaks are underestimated compared to the experimental data, especially the one at 1.74 Å, and so are the peaks of the partial functions. Thus, the related peaks in the radial distribution function $J(r)=4\pi r^2\rho(r)$ are also too small. The areas under these peaks are proportional to the coordination number, and Schempp *et al.* obtained the areas by fitting two Gaussian curves for Si-N and Si-C with centers corresponding to the bond lengths in Table I to the main peak. Having a higher peak, this must lead to a larger coordination number, especially for Si-N which gives the main contribution to this peak in the total function. In addition, the C-C contribution at 1.40 Å which has not been taken into account in the fit also causes a smaller Si-N peak (see Fig. 6). In this way the discrepancy between the experimental and calculated coordination numbers k_{SiN} and k_{NSi} can be understood, above all considering also that $k_{NSi}=3.6$ is just too large for an average coordination number of nitrogen favorably bonded in Si_3N_4 tetrahedra.

C. Phase-separated layered amorphous model

Again, based on the idea of the phase separation, another starting structure was created. It was prepared as the one for the model PSC with the only difference that now the carbon atoms were inserted that way that only one carbon-rich domain exists. This model, too, includes 224 atoms in the periodic supercell of the same composition and density as the

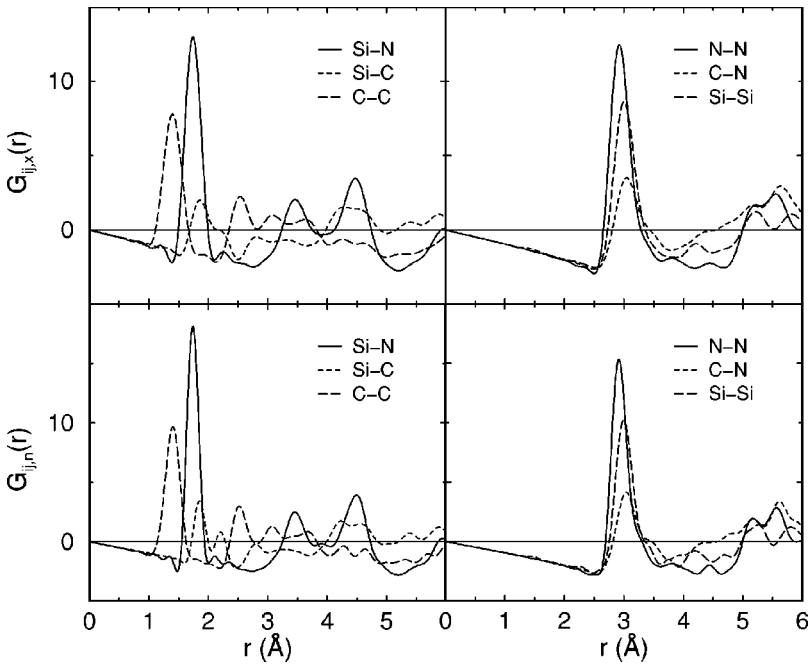

FIG. 6. Calculated partial pair correlation functions of the phase-separated clustered amorphous model PSC from x-ray (upper panel) and neutron (lower panel) diffraction.

other models. After application of the MD simulation process, the structure displayed in Fig. 7 was obtained.

In contrast to the first phase-separated model PSC, the carbon atoms are arranged in more chainlike structures forming an amorphous layer throughout the whole supercell. Within the layer and at the edges of it, silicon atoms are located, building a small SiC phase which mediates the transition to the amorphous Si_3N_4 phase.

The average coordination numbers given in Table I differ only in a slightly larger coordination of Si-C and C-Si from the ones of the PSC model, while the bond lengths are almost the same. Furthermore, the total structure factors, shown in Fig. 8, not only agree very well with the experimental ones, but are also nearly identical with the total structure factors of the model PSC. The two peaks in the range of $5-10$ Å^{-1} in $S_x(q)$ and $S_n(q)$ match the experimental curves even slightly better.

Looking at the total pair correlation functions (see Fig. 9), there is a strong resemblance between the ones obtained from these structure factors by Fourier transformation and the experimental ones from x-ray and neutron diffraction as

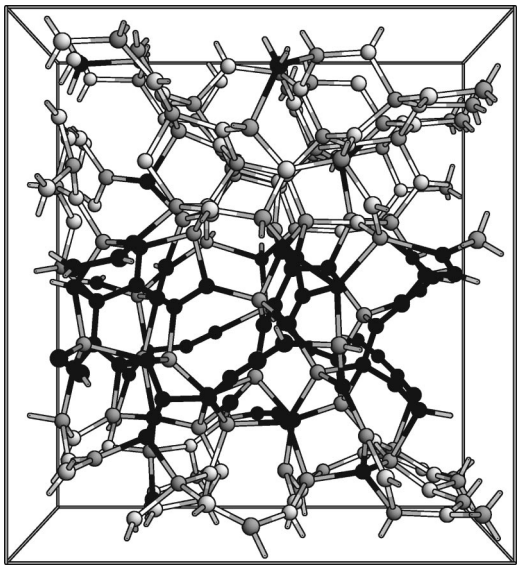

FIG. 7. Structure of the phase-separated layered amorphous model PSL. Carbon atoms are shown as black spheres, silicon as dark gray ones, and nitrogen as white ones.

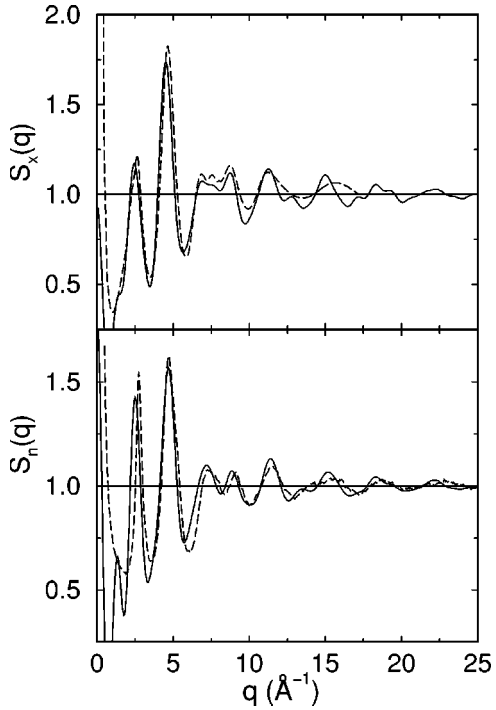

FIG. 8. Calculated total structure factors of the phase-separated layered amorphous model PSL (solid line) and experimental ones of the ceramic produced by Schempp *et al.* (Ref. 3) (dashed line) from x-ray (upper panel) and neutron (lower panel) diffraction.

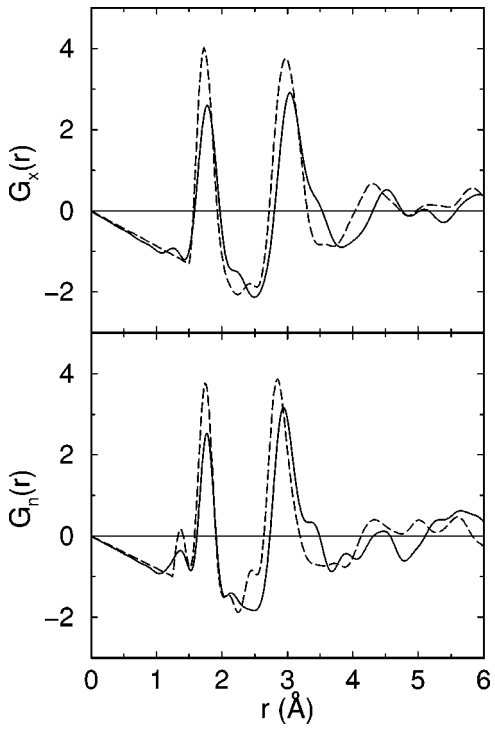

FIG. 9. Calculated total pair correlation function of the phase-separated layered amorphous model PSL (solid line) and experimental ones of the ceramic produced by Schempp *et al.* (Ref. 3) (dashed line) from x-ray (upper panel) and neutron (lower panel) diffraction.

well as between them and the $G_x(r)$ and $G_n(r)$ of the PSC model. The first hint of the different atomic distributions of the two amorphous models can be found in the region from $r=4$ Å upwards, where peak positions and heights slightly vary.

The difference reveals itself more clearly considering the partial pair correlation functions shown in Fig. 10. While the Si-N correlation is almost the same as for the PSC model because of the similar local environment of Si in both structures, the first C-C peak at 1.38 Å is slightly smaller but broader due to the more chainlike structure of the amorphous carbon layer. In addition, there appear two C-C peaks at 3.29 Å and 3.84 Å for neutron scattering which cause the small broadening at the right side of the peak at 2.94 Å and the small peak at 3.90 Å in $G_n(r)$. In the region beyond 3 Å, the C-C correlation is even stronger than it is for the PSC model with the carbon clusters due to the more extended carbon layer here. On the other hand, the Si-C correlation is less strong from 4 Å on, compared to the PSC model. This results from constraining these correlations to only one layer in this phase-separated layered amorphous model PSL while the carbon clusters are distributed throughout the whole structure in the PSC model. Nevertheless, considering the weighting factors, the assignment of the main peaks in the total pair correlation function remains the same as for the PSC model. Only the peak at 4.47 Å is slightly smaller for the PSL model consisting mainly of the Si-N correlation instead of Si-N and Si-C for PSC.

As expected, the Si-Si curve does not change noticeable. In both models the silicon atoms are distributed very similar throughout the structure. Therefore, taking into account the large weighting factor of Si-Si, the peak at 3.04 Å in the total $G_x(r)$ of PSL is almost identical with the corresponding one for PSC. The next-nearest-neighbor correlation of N-N at 2.90 Å increases due to the continous layered structure of the amorphous Si_3N_4 in comparison to the cluster-interrupted structure of PSC. The same holds for the higher N-N peak at 5.28 Å. The decrease of the C-N correlation is due to the same effect. Having only one central region of amorphous carbon, there are less nitrogen atoms in a distance of 3.02 Å from it. Thus, regarding the weighting factors for neutron

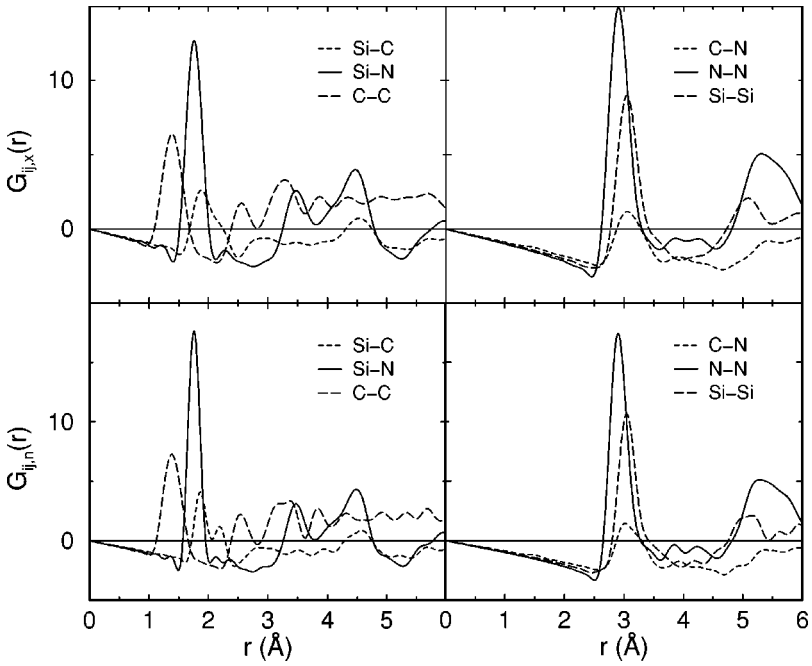

FIG. 10. Calculated partial pair correlation functions of the phase-separated layered amorphous model PSL from x-ray (upper panel) and neutron (lower panel) diffraction.

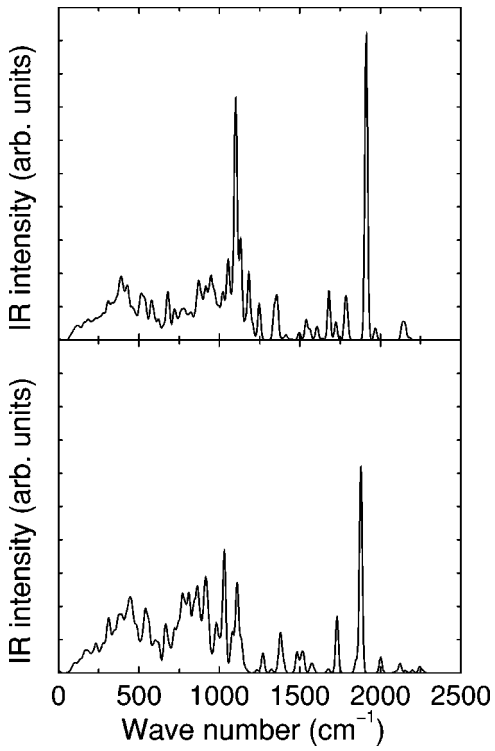

FIG. 11. Calculated infrared intensities of the phase-separated amorphous models PSC (upper panel) and PSL (lower panel).

scattering, the larger contribution of N-N to the total pair correlation function is compensated by the smaller amount of Si-C correlations. In this way the total pair correlation function of PSL is almost identical with PSC in the region around 3 Å.

V. INFRARED SPECTRA

For further comparison of the two phase-separated models and to supplement the characterization, we had a look at the infrared (IR) intensities of the two structures (see Fig. 11). Concerning these spectra, clear differences between the two structures become obvious. Although the overall shape for both models still remains similar, they can be well distinguished, especially by the different peak positions and heights in the range from 650 cm^{-1} to 1250 cm^{-1} and around 1750 cm^{-1}. Since the latter region is dominated by contributions of short C-C bonds, the differences in the IR intensity are clearly due to the different carbon clustering in the structures.

VI. CONCLUSION

We have shown that the precursor-derived amorphous ceramic $Si_{37}C_{32}N_{31}$ produced by Schempp *et al.* definitely does not consist of a homogeneous distribution of atom types. Rather, a phase separation on the atomic scale into amorphous Si_3N_4, amorphous SiC, and amorphous carbon exists in the final ceramic product. This is in good agreement with the experimental results and the position of this ceramic in the ternary phase diagram of Si-C-N between the quasibinary lines of Si_3N_4-C and Si_3N_4-SiC.[3]

We have proposed two possible model structures, both including phase separation, but with different structural arrangements. One model includes carbon clusters of six to nine atoms forming ringlike structures, each surrounded by an amorphous SiC layer, which are embedded in the amorphous Si_3N_4 phase. The other model consists of a more chainlike layered amorphous carbon phase extended throughout the whole supercell structure with a small interface of SiC at the edges followed by amorphous Si_3N_4.

This phase separation, in particular the formation of carbon clusters, is thought to retard the crystallization process by hindering the thermal diffusion of the other atoms upon annealing and in this way to improve the temperature stability.

Both structures show almost identical bond lengths, coordination numbers, total structure factors, and total pair correlation functions, being in very good agreement with the corresponding experimental data from x-ray and neutron diffraction. The difference in the atomic distribution can only be seen from the calculated partial pair correlations and the IR spectra. Therefore, none of these two models can be given preference concerning the experimental results and in turn should stimulate further investigations.

However, regarding the restricted model size of approxiamtely 14 Å and for example the resolution limit of 20 Å of the ESI technique, the long-range order of both periodic structures will still appear as an amorphous and homogeneous distribution of all involved atom types. Thus, this is consistent with the ESI results of Bill *et al.*[8] who found the same homogeneous distribution of Si, N, and C in their precursor-derived material on a range of severaly 1000 Å.

ACKNOWLEDGMENTS

The authors are indebted to the Deutsche Forschungsgemeinschaft for financial support from the DFG Schwerpunktprogramm ''Precursorkeramik''. M.A. would like to thank G. Jungnickel for useful and stimulating discussions and P. Lamparter for providing the experimental total structure factors and total pair correlation functions.

*Electronic address: amkreutz@phys.upb.de

[1] R. Riedel, G. Passing, H. Schönfelder, and R.J. Brook, Nature (London) **355**, 714 (1992).

[2] P. Greil, Adv. Eng. Mat. **6**, 339 (2000).

[3] S. Schempp, J. Dürr, P. Lamparter, J. Bill, and F. Aldinger, Z. Naturforsch., A: Phys. Sci. **53**, 127 (1998).

[4] H. Uhlig, M. Frieß, J. Dürr, R. Bellissent, H.-P. Lamparter, F. Aldinger, and S. Steeb, Z. Naturforsch., A: Phys. Sci. **51**, 1179 (1996).

[5] J. Seitz, J. Bill, N. Egger, and F. Aldinger, J. Eur. Ceram. Soc **16**, 885 (1996).

[6] J. Dürr, P. Lamparter, J. Bill, S. Steeb, and F. Aldinger, J. Non-Cryst. Solids **223-234**, 155 (1998).

[7] R. Riedel, F.A.H. Kleebe, and H. Schönfelder, Nature (London) **374**, 526 (1995).

[8] J. Bill, J. Seitz, G. Thurn, J. Dürr, J. Canel, B.Z. Janos, A. Jalowiecki, D. Sauter, S. Schempp, H.P. Lamparter, J. Mayer, and F. Aldinger, Phys. Status Solidi A **166**, 269 (1998).

[9] R.L. McGreevy and L. Pusztai, Mol. Simul. **1**, 359 (1988).
[10] J. Tersoff, Phys. Rev. B **39**, 5566 (1989).
[11] K. Matsunaga, Y. Iwamoto, C.A.J. Fisher, and H. Matsubara, J. Ceram. Soc. Jpn. **107**, 1025 (1999).
[12] D. Porezag, T. Frauenheim, T. Köhler, G. Seifert, and R. Kaschner, Phys. Rev. B **51**, 12 947 (1995).
[13] T. Frauenheim, F. Weich, T. Köhler, S. Uhlmann, D. Porezag, and G. Seifert, Phys. Rev. B **52**, 11 492 (1995).
[14] J. Widany, T. Frauenheim, T. Köhler, M. Sternberg, D. Porezag, G. Jungnickel, and G. Seifert, Phys. Rev. B **53**, 4443 (1996).
[15] G. Seifert, D. Porezag, and T. Frauenheim, Int. J. Quantum Chem. **58**, 185 (1996).
[16] T.E. Faber and J.M. Ziman, Philos. Mag. **11**, 153 (1965).
[17] S.R. Elliott, *Physics of Amorphous Materials*, 2nd ed. (Longman Scientific & Technical, Harlow, Essex, 1983).
[18] E. Lorch, J. Phys. C **2**, 229 (1969).
[19] F. Jungnickel, Ph.D. thesis, Technische Universität Chemnitz, Fakultät für Mathematik und Naturwissenschaften, Chemnitz, 1990.
[20] D.M. Teter and R.J. Hemley, Science **271**, 53 (1996).
[21] V. Hietschold and G. Seifert, Phys. Status Solidi B **129**, K163 (1985).
[22] R.A. Street, *Hydrogenated Amorphous Silicon* (Cambridge University Press, Cambridge, England, 1991).
[23] P.H. Gaskell, *Materials Science and Technology* (Verlag Chemie, Weinheim,1991), Vol. 9, p. 230.
[24] G. Jungnickel, Ph.D. thesis, Technische Universität Chemnitz, Fakultät für Naturwissenschaften, Chemnitz, 1993.
[25] S.N. Ruddlesden and P. Popper, Acta Crystallogr. **11**, 465 (1958).
[26] P.T.B. Shaeffer, Acta Crystallogr., Sect. B: Struct. Crystallogr. Cryst. Chem. **25**, 477 (1969).
[27] This is tested by the authors even using higher temperatures up to 4000 K, longer time periods up to 10 ps, or other pyrolysis regimes for the MD than the given one. All these attempts lead to a homogeneous distribution of all atom types throughout the structure. The best result compared with the experimental data was obtained with the mentioned MD scheme with 1000 K. The others did not result in any improvement of the model structure considering the experimental findings or were even worse, especially the ones with higher temperatures.